

Citation for published version:

Ryan D. Himes, Nikolai Smolin, Andreas Kukol, Julie Bossuyt, Donald M. Bers, and Seth L. Robia, 'L30A Mutation of Phospholemman Mimics Effects of Cardiac Glycosides in Isolated Cardiomyocytes', *Biochemistry*, Vol. 55 (44): 6196-6204, October 2016.

DOI:

<https://doi.org/10.1021/acs.biochem.6b00633>

Document Version:

This is the Accepted Manuscript version.

The version in the University of Hertfordshire Research Archive may differ from the final published version.

Copyright and Reuse:

© 2016 American Chemical Society.

This manuscript version is made available for non-commercial purposes and in accordance to the terms of American Chemical Society, see <http://pubs.acs.org/ethics>

Enquiries

If you believe this document infringes copyright, please contact the Research & Scholarly Communications Team at rsc@herts.ac.uk

L30A mutation of phospholemman mimics effects of cardiac glycosides in isolated cardiomyocytes

Ryan D. Himes¹, Nikolai Smolin¹, Andreas Kukol², Julie Bossuyt³, Donald M. Bers³ and Seth L. Robia^{1*};

¹Department of Cell and Molecular Physiology, Loyola University Chicago, Maywood, IL, USA

²School of Life and Medical Sciences, University of Hertfordshire, Hatfield, UK

³Department of Pharmacology, The University of California, Davis, CA, USA

***To whom correspondence should be addressed:** Seth L. Robia, PhD; Department of Cell and Molecular Physiology, Loyola University Chicago, 2160 South First Avenue, Maywood, IL 60153, USA; Phone: (708) 216-2522, Email: srobia@luc.edu

Donald M. Bers, PhD; Department of Pharmacology, The University of California, Genome Building Room 3513, Davis, CA 95616; Phone: 530-752-6517, Email: dmbers@ucdavis.edu; Julie Bossuyt, PhD; Department of Pharmacology, The University of California, 451 Health Sciences Drive, Genome Building Room 3617, Davis, CA 95616; Phone: 530-754-7419, Email: jbossuyt@ucdavis.edu; Andreas Kukol, PhD; School of Life and Medical Sciences, University of Hertfordshire, College Lane, Hatfield AL10 9AB, UK; Phone: +44-(0)1707 284 543 Email: a.kukol@herts.ac.uk; Ryan D. Himes, PhD; present address: Dept. of Biological Sciences, Olivet Nazarene University, One University Ave, Bourbonnais, IL 60914, Email: rdhimes@olivet.edu.

Sources of funding: This work was supported by American Heart Association predoctoral fellowship 15PRE22930025 to RDH and National Institutes of Health R01 grant HL092321 to SLR. This work used the Extreme Science and Engineering Discovery Environment (XSEDE), which is supported by National Science Foundation grant number OCI-1053575. This research was supported by equipment and facilities provided by National Institute of Health grant "Loyola Research Computing Core" 1G20RR030939.

Keywords:

heart failure, phospholemman, Na,K-ATPase, FRET, homotransfer FRET, cardiac glycosides, gene therapy, cardiac muscle, excitation-contraction coupling

Abbreviations: PLM (phospholemman), NKA (Na,K-ATPase), PLB (phospholamban), SERCA (sarco/endoplasmic reticulum calcium-ATPase), NCX (sodium-calcium exchanger), FRET (Förster Resonance Energy Transfer), Cit (citrine), ECFP (Enhanced Cyan Fluorescent Protein), HEK (human embryonic kidney), ER (endoplasmic reticulum), SR (sarcoplasmic reticulum), MD (molecular dynamics), PBS (phosphate buffered saline), FBS (fetal bovine serum), DMEM (Dulbecco's Modified Eagle's medium), SEM (standard error of the mean), FWHM (full width at half maximum).

ABSTRACT

To determine if mutations made to PLM could increase PLM-NKA binding we performed scanning mutagenesis of the transmembrane domain of PLM and measured FRET between each mutant and NKA. We observed increased binding to NKA for several PLM mutants compared to WT, including L27A, L30A, and I32A. In isolated cardiomyocytes, overexpression of WT PLM increased the amplitude of the Ca^{2+} transient compared to GFP control. Ca^{2+} transient amplitude was further increased by L30A PLM overexpression. L30A mutation also delayed Ca^{2+} extrusion and increased the duration of cardiomyocyte contraction. This mimics aspects of the effect of cardiac glycosides, which are known to increase contractility through inhibition of NKA. No significant differences between WT and L30A PLM expressing myocytes were observed after treatment with isoproterenol, suggesting that the superinhibitory effects of L30A are reversible with β -adrenergic stimulation. We also observed a decrease in PLM tetramerization with L30A compared to WT using FRET, suggesting that L30 is an important residue for mediating PLM-PLM binding. MD simulations revealed that the potential energy of the L30A tetramer is greater than the WT, and that the transmembrane alpha helix is distorted by the mutation. The results implicate PLM residue L30 as an important determinant of PLM tetramerization and of functional inhibition of NKA by PLM.

Heart failure, defined as insufficient cardiac output to meet the demands of the body^{1,2}, is one of the leading causes of morbidity and mortality in the US³. Cardiac glycosides, such as digitalis, have been used to treat heart failure for centuries⁴⁻⁶. They act by selectively binding to the Na,K-ATPase (NKA) on the outside of cardiomyocytes, inhibiting pump activity⁷. This leads to an increase in cytosolic sodium concentration, $[Na^+]_i$, which in turn inhibits the Ca^{2+} extrusion activity of the sodium-calcium exchanger (NCX)⁸. Decreased Ca^{2+} extrusion prolongs the contraction and increases SR Ca^{2+} load, increasing contractility⁹. However, the therapeutic window of glycosides is narrow, as high doses lead to overload of Ca^{2+} in the SR, Ca^{2+} leak, and arrhythmogenesis⁵. In the event of an overdose, treatment with antibody to the drug is necessary, as drug clearance is otherwise relatively slow (the half-life of digoxin is 20-50 hours, for example)⁶.

NKA is also regulated by the endogenous peptide phospholemman (PLM, also referred to as FXYD1)^{10,11}, and in contrast to cardiac glycosides, this inhibition is dynamically regulated by the cell. PLM is phosphorylated on its C-terminus by PKA and PKC in response to adrenergic stimulation and this phosphorylation causes relief of inhibition of NKA (**Fig. 1A**)¹². Phosphorylation may also modulate a parallel regulatory interaction of PLM with other Ca-handling proteins, such as NCX¹³⁻¹⁵. Phosphorylation has been shown to increase the formation of PLM tetramers (**Fig. 1B**), which are not believed to interact with NKA¹⁶⁻¹⁹. While monomeric PLM reduces the affinity of NKA for sodium ions, it has little to no effect on the maximum transport rate (V_{max}) of NKA²⁰. Therefore, inhibition by PLM can be overcome at high $[Na^+]_i$. For these reasons, we theorized that mutations made to PLM that increase binding to and inhibition of NKA (superinhibitory PLM) could be superior inotropic agents compared to cardiac glycosides.

Whether PLM mutations could be positively inotropic (enhancing cardiac contractions) has not been extensively studied prior to the work in this publication. Here we sought to test the following hypothesis: a mutation made to the transmembrane domain of PLM will increase PLM-NKA binding, leading to downstream positive inotropy by inhibiting Na^+ extrusion and consequently reducing Ca^{2+} efflux via NCX, mimicking the action of cardiac glycosides. Our approach was to use FRET to screen 19

PLM mutants and test candidates for functional effects in isolated cardiomyocytes. We also monitored the effect of mutation on PLM tetramerization to test whether oligomerization influences PLM-NKA binding.

EXPERIMENTAL PROCEDURES

Molecular biology and cell culture: PLM fused to Citrine (Cit) was previously described. This construct has PLM fused at the C-terminus to the N-terminus of the yellow fluorescent protein Cit with a 21 residue linker¹². Individual alanine substitutions were created by site-directed mutagenesis. Adenoviruses containing WT and mutant PLM-Cit DNA sequences were generated using the AdEasy kit (Stratagene) as previously described²¹. All DNA sequences were verified by sequencing (ACGT, Inc.). AAV-293 cells stably expressing enhanced cyan fluorescent protein (ECFP) tagged to the N-terminus of NKA²² were maintained in Dulbecco's Modified Eagle's medium (DMEM) + 10% FBS. Cells were transfected with 1 µg of PLM-Cit plasmid DNA per 60 mm dish of 250,000 cells (Turbofect, ThermoFisher) according to manufacturer instructions.

Acceptor sensitization FRET and anisotropy measurements: 24 h post-transfection, cells were trypsinized and plated at a density of 150,000 cells/well in a 4-well glass-bottom chamber (MatTek). Cells were incubated for 90 min at 37°C in DMEM + 10% FBS, and then were washed two times with PBS, followed by loading with 2 µg/mL wheat germ agglutinin (WGA) Alexa Fluor 594 (Molecular Probes). WGA was applied to the cells for 3 min, then the cells were washed three times with PBS. Images of cells were acquired using a Nikon inverted microscope with 40X air objective. Acceptor sensitization FRET was used to measure binding between ECFP-NKA and each PLM-Cit construct. For each acquisition field, a set of four images was taken to capture the fluorescence of ECFP, Cit, FRET, and WGA Alexa Fluor 594, with exposure times of 2000, 50, 500, and 300 ms respectively. For the ECFP, Cit, and WGA images, the specific fluorophore was excited and its emission was captured, whereas for the FRET image, ECFP was excited and Cit emission was captured. Then the stage was automatically shifted so that a new field was in focus, and the imaging was repeated. For each PLM construct 130 fields

were imaged in rapid succession using automated stage movements. Focus on the cells was maintained using a Nikon PFS feedback system.

To quantify PLM-PLM binding, the stage was reset back to the initial position, and image scanning was repeated, this time using polarization filters in order to measure fluorescence anisotropy of PLM-Cit. If the PLM-Cit peptides are in close proximity in the membrane, homotransfer FRET can occur between neighboring Cit fluorophores²³. This energy transfer decreases the polarization of emitted fluorescence, which is quantified as a decrease in fluorescence anisotropy. To measure the anisotropy of PLM-Cit, vertically polarized excitation light (wavelength = 504/12 nm) was used and then emission was captured with either a vertical (I_{parallel}) or a horizontal ($I_{\text{perpendicular}}$) polarizing filter in the emission light path. Both of these images were acquired with an exposure time of 1000 ms.

For each field the WGA Alexa Fluor 594 image, which displayed fluorescence only at the plasma membrane of each cell, was used to generate a “mask” that was then applied to all other images. This was done using a no-neighbors deconvolution algorithm (Metamorph) performed on the WGA images. Masks of just the plasma membrane of each cell were then applied to all the other images in order to reduce the contribution of any intracellular expression of fluorescent protein constructs. This allowed for the calculation of acceptor sensitization and anisotropy solely at the plasma membrane, where PLM-NKA and PLM-PLM binding is relevant.

For each cell, acceptor sensitization FRET was calculated according to the formula:

$$\text{FRET Efficiency (\%)} = 100 * (I_{\text{FRET}} - aI_{\text{Cit}} - dI_{\text{ECFP}}) / (I_{\text{FRET}} - aI_{\text{Cit}} - dI_{\text{ECFP}} + GI_{\text{ECFP}}),$$

where I_{FRET} , I_{Cit} , and I_{ECFP} are the average intensities of each cell in the FRET, Cit, and ECFP images, respectively, ‘a’ is the acceptor cross-excitation coefficient, ‘d’ is the donor bleed-through coefficient, and G is the ratio of sensitized emission to donor emission for a standard FRET construct (control donor-acceptor fusion)²⁴. For the experiments performed in this manuscript, a = 0.091, d = 0.83, and G = 4.6.

Anisotropy was calculated according to the formula:

$$r = (I_{\text{parallel}} - I_{\text{perpendicular}}) / (I_{\text{parallel}} + 2I_{\text{perpendicular}}),$$

where r is the average anisotropy of each cell.

Calculation of PLM-PLM and PLM-NKA binding affinities: Average acceptor sensitization FRET and anisotropy values were plotted against the PLM-Cit fluorescence value of each cell (24). The data were fit by Hill functions in Origin software. Acceptor sensitization FRET was well described by the following relationship:

$$\text{FRET Efficiency (\%)} = c + ((\text{FRET}_{\text{max}} - c) * [\text{Protein}]^n) / (K_{\text{D}2}^n + [\text{Protein}]^n)$$

where c is the FRET of the unbound fluorescent proteins, and FRET_{max} is the FRET of the fully bound regulatory complex; n is the Hill coefficient, and $[\text{Protein}]$ is the average intensity of Cit for each cell in arbitrary units, taken to be an index of the concentration of PLM. $K_{\text{D}2}$ is the dissociation constant for the PLM-NKA complex. Homotransfer FRET was evaluated by the following relationship:

$$\text{anisotropy (r)} = r_0 + ((r_n - r_0) * [\text{Protein}]^n) / (K_{\text{D}1}^n + [\text{Protein}]^n)$$

where r_n is the anisotropy of the fully bound PLM tetramer, and $K_{\text{D}1}$ is the dissociation constant. The value r_0 is the inherent anisotropy of unbound fluorescent proteins; however estimation of anisotropy for very dim (low expressing) cells was complicated by a variable background of highly polarized scattered light. Thus we do not consider values of r_0 to be informative here. For each mutant PLM, four separate binding curves from four different transfections were globally fit, sharing all parameters except for K_{D} . These four pairs of K_{D} values were then averaged and plotted with associated SEM.

Molecular Dynamics (MD) Simulations of WT and L30A PLM tetramers

To compare the energetics of WT and L30A PLM oligomers we performed molecular dynamics simulations of a model of the PLM tetramer (Cluster 1)²⁵ in GROMACS^{26, 27}, using the CHARMM 36²⁸ force field and TIP3P²⁹ water model. Energy minimization was performed on the PLM tetramers using the steepest descent method for 1000 steps, then the transmembrane helices of each model were inserted into a POPC lipid bilayer, removing overlapping lipids. The structure was solvated in a water box, with 150 mM Na⁺ and Cl⁻ ions added to neutralize the charge of the system. The Particle Mesh Ewald method^{30, 31} was used to calculate the long-range electrostatic interactions, with a cut-off of 12 Å for short-range interactions. Van der Waals interactions were reduced to zero by switch truncation applied from 8 to 12 Å. To heat the system from 0 K to the target temperature (300 K) and reach the target pressure (1 bar), the

Berendsen method was used with relaxation times of 0.1 ps³². After 1 ns equilibration, the production run was performed in the NPT ensemble using the Nose-Hoover thermostat^{33, 34} and the Parrinello-Rahman barostat^{35, 36} with relaxation times of 1.0 ps. Three independent production runs were carried out for 50 ns for each variant with an integration time step of 2 fs.

Physiological measurements in cardiomyocytes: Rabbit ventricular myocytes were isolated as previously described³⁷. Cells were transferred to laminin-coated 14 mm cover slips (MatTek) and incubated for one hour in PC-1 medium (Lotran, Inc.). Virus was added to the cells at a multiplicity of infection of 500 virus particles per cell³⁷. Cells were incubated and paced with 10V, 5 ms duration pulses, at a frequency of 0.1 Hz for 18 h.

Cells were visualized using confocal microscopy in order to observe the expression and localization of the PLM-Cit. Cells were then washed twice with Tyrode solution and loaded with 10 μ M Indo-1 acetoxymethyl ester for 20 min, followed by three more washes. Measurements were made with cells in the presence of either Tyrode solution alone, or 20 nM isoproterenol in Tyrode solution. Myocytes were stimulated using 30V, 2 ms duration pulses, and 0.5 Hz frequency³⁷. Myocytes were measured only if they were contracting longitudinally, were properly adhered to the laminin-coated cover slip, and were not touching other cells. Using an IonOptix system, average sarcomere length and Indo-1 fluorescence were simultaneously measured. Ten pulses were measured for each cell. The resulting traces were then averaged together and fit using IonOptix software.

Statistics: Data were plotted as mean \pm SEM. Mutants were compared to WT using Student's unpaired T-test, with significance being noted at $p < 0.05$.

RESULTS

Effects of PLM mutations on PLM-PLM and PLM-NKA FRET: Transiently transfected HEK cells expressing fluorescently-tagged PLM mutants showed intracellular fluorescence near the nucleus (likely in the endoplasmic reticulum) and in the plasma membrane (**Fig. 1C**). To specifically quantify the fluorescence of PLM/NKA localized in the plasma membrane and exclude intracellular fluorescence, we

generated a selection mask from images of WGA labeled with Alexa Fluor 594 (**Fig. 1C**). We quantified PLM-NKA binding by measuring FRET between ECFP-NKA and each mutant PLM-Cit construct. The average FRET efficiency of each cell was compared to the intensity of Cit fluorescence, which was taken as an index of the expression of acceptor-labeled PLM. As previously observed¹⁸, FRET increased with PLM-Cit toward a maximum (**Fig. 1D**). The data are consistent with increased binding of PLM to NKA with increasing membrane protein concentration.

PLM-PLM binding was quantified by homotransfer FRET measured from Cit fluorescence anisotropy. Cit has a high intrinsic fluorescence anisotropy and we observed decreasing anisotropy with increasing expression of PLM (**Fig. 1E**), consistent with increasing homotransfer FRET within the PLM tetramer. Acceptor sensitization/homotransfer FRET binding curves were analyzed by Hill function fitting, yielding the relative dissociation constants for the respective protein complexes: K_D1 for the PLM tetramer, and K_D2 for the PLM-NKA complex (**Fig. 2**). Fit results are provided in **Table 1**. A comparison of K_D values of PLM mutants (**Fig. 2**) reveals differences from WT (indicated by *, $p < 0.05$). All PLM mutants showed robust homotransfer and acceptor sensitization FRET, indicating that all were capable of oligomerizing and binding to NKA (**Table 1**).

As we previously observed^{12, 18}, a phosphomimetic mutant of PLM with key phosphorylation sites S63 and S68 replaced with glutamate showed increased oligomerization compared to WT or a nonphosphorylatable (S63A/S68A) mutant of PLM. In that previous study, the increased oligomerization of S63E/S68E was matched by a decrease in binding to NKA (increased K_D2)¹⁸. Here we also observed an increased K_D2 relative to S63A/S68A ($p < .0001$) (though the value was not statistically distinguishable from WT, $p = .067$). The observed decrease in binding to NKA of the phosphomimetic mutant relative to nonphosphorylatable PLM confirms our previous conclusion that PLM phosphorylation reduces the apparent affinity of the interaction but does not abolish binding¹⁸. The apparent persistence of the regulatory complex after phosphorylation is also consistent with a recent study by Mishra et al. in which they showed protection of NKA from heat denaturation by both WT and phosphomimetic PLM³⁸. Based on that apparent reciprocal relationship of K_D1 and K_D2 (increased oligomerization of S63E/S68E

matched by a decrease in binding to NKA)¹⁸ we previously hypothesized that oligomerization of PLM substantially limits the availability of the monomeric form. In a similar fashion, phospholamban (PLB) oligomerization is thought to determine its potency for regulating the sarco/endoplasmic reticulum calcium-ATPase (SERCA)³⁹⁻⁴¹. However, in the present more extensive survey of PLM transmembrane domain mutations we did not observe a strong link between PLM oligomerization and PLM-NKA binding. In particular, many mutants showed enhanced NKA-binding despite apparently increased (or unaltered) oligomerization affinity. Mid-depth transmembrane domain alanine substitution mutants between I23A to S37A significantly increased binding to NKA, irrespective of their propensity for oligomerization. The data suggest that the relative availability of monomer is not the sole determinant of NKA-binding. One mutant that did conform to the expected inverse relationship of K_{D1} and K_{D2} was L30A PLM, which exhibited nearly 4-fold higher K_{D1} compared to WT and a ~2 fold lower K_{D2} . It is not clear whether the increased binding to NKA is due solely to increased availability of monomer, or reflects increased intrinsic affinity of monomer for NKA. It may be that oligomerization and the NKA-PLM interaction are both independently affected by L30A.

Effect of L30A mutation on PLM tetramer energetics: To identify possible structural mechanisms of depolymerization of PLM by L30A, we examined a model of the PLM tetramer generated in a previous study using site-specific infrared spectroscopy and experimentally constrained high throughput MD simulations¹⁶. Here we performed 50 ns MD simulations of model “Cluster 1”, which was selected from 6 alternative models on the basis of the relative orientation of protomers in the tetramer. In this model L30 protruded into the center of the tetramer, and we hypothesized that mutation of this residue could alter the stability of the complex. The quaternary arrangement of transmembrane helices is shown in Fig. 3A, viewed along the membrane normal axis from the cytoplasmic side, with the leu or ala at position 30 highlighted in blue. The relative positions of the transmembrane helices were stable over 50 ns for WT PLM, but we observed significant distortion of the L30A structure within the first few ns of the simulation (Fig. 3A), with some intrusion of lipid into the space created by the replacement of the bulky Leu sidechain with the smaller Ala. In addition, the consequence of loss of

contacts between the L30 sidechains and adjacent protomers was visible within the first 10 ns of the simulation as a difference in the potential energy between the WT (-2842 ± 172 kJ/mol) and mutant (-2676 ± 174 kJ/mol). This difference became more extreme over the course of the 50 ns trajectory. Fig. 3B shows histograms of the binding energy values calculated at the beginning of the simulation (0-10 ns, thin lines) and the end of the simulation (40-50 ns, thick lines) for WT and L30A. WT PLM became more stable over time, assuming a configuration with a more negative potential energy (-2970 ± 246 kJ/mol) (Fig. 3B, thick black line). In contrast, the evolution of the L30A mutant resulted in a less negative potential energy of the tetramer at the end of the simulation (-2536 ± 160 kJ/mol). Overall, the less negative potential energy of the mutant relative to the WT, which worsened over time, suggested instability of the Cluster 1 tetramer structure after L30A mutation. The molecular dynamics simulations are compatible with the decrease in tetramer affinity (increase in K_D) observed for L30A PLM (Fig. 2A). We also examined an alternative model, "Cluster 6", which was previously identified as the structure in closest agreement with infrared spectroscopy measurements based on synthetic transmembrane peptides in dimyristoyl-phosphocholine lipids (31). A 10 ns simulation showed that compared to Cluster 1 the calculated potential energy of the WT Cluster 6 structure was somewhat less negative (-2753 ± 242 kJ/mol). Nevertheless, Cluster 6 potential energy was also increased by the L30A mutation (-2576 ± 212 kJ/mol).

Functional effects of PLM mutations: The physiological effect of NKA inhibition by cardiac glycosides is to increase intracellular Na^+ , resulting in decreased extrusion of Ca^{2+} by NCX and enhanced cardiac contraction⁴²⁻⁴⁵. We hypothesized that increased NKA binding by inhibitory PLM would have a similar effect. To evaluate this possible mechanism, we selected three candidate mutants (L27A, L30A and I32A) that showed increased apparent affinity for NKA (**Fig. 2B**). These PLM mutants were overexpressed in isolated rabbit ventricular myocytes using adenoviral delivery. After 24 h, confocal microscopy revealed that the PLM-Cit fluorescence was localized in the perinuclear region and in the plasma membrane (**Fig. 4A**). The plasma membrane fraction co-localized with Alexa Fluor 594 WGA in

a T-tubular pattern (**Fig. 4A**). Cells were electrically paced at 0.5 Hz to measure Ca^{2+} release (with Indo-1) and cell shortening. Addition of exogenous WT PLM-Cit was associated with a prolongation of the Ca^{2+} transient (increased decay time constant τ) and increased transient amplitude compared to non-fusion GFP controls (**Fig. 4B**). Importantly, this result suggests that not all pumps are bound or regulated by PLM in rabbit cardiomyocytes, and that physiological inhibition of NKA may be increased by delivery of PLM to the unoccupied regulatory sites. This is in contrast to observations of the related P-type ATPase, SERCA, which appears to be saturated by endogenous PLB in the rabbit heart. A study of PLB-overexpressing rabbits revealed no phenotype ⁴⁶.

To determine the effect of PLM mutations, we compared Ca^{2+} transients of cells expressing candidate mutants to cells expressing exogenous WT PLM-Cit. Relative to WT, L30A showed the most profound effect, prolonging the Ca^{2+} transient and modestly increasing Ca^{2+} transient amplitude (**Fig. 4C, H**). L27A and I32A effects were similar to WT (**Fig. 4H-J**). The effects of control GFP or PLM mutant overexpression on Ca^{2+} handling parameters are summarized in **Fig. 4H-J**, all normalized to WT. To determine whether cells expressing superinhibitory L30A PLM could respond to adrenergic stress we applied 20 nM isoproterenol and observed positive inotropy (enhanced contraction) and lusitropy (enhanced relaxation). After isoproterenol treatment L30A PLM-expressing cells showed no significant difference from cells expressing exogenous WT PLM (**Fig. 4D,G**). That we observed no residual broadening of the Ca^{2+} transient suggests that NKA superinhibition by L30A was relieved by activation of β -adrenergic pathways.

Despite increased Ca^{2+} transient amplitude, we did not observe a significant increase in fractional shortening (**Fig. 4E, F, K**). However, we noted that the resting sarcomere length of the cultured cardiomyocytes was already quite short, possibly limiting further contraction. Instead, enhanced Ca^{2+} transients manifested as a longer contraction phase (**Fig. 4E-F**), as measured by a significantly larger full width at half maximum (FWHM) and increased relaxation time constant (**Fig. 4L-M**). The effects of control GFP or PLM mutant overexpression on cell shortening parameters are summarized in **Fig. 4K-M**,

all normalized to WT. The comprehensive results of the experiments comparing WT to L30A PLM under baseline conditions are summarized in **Tables 2** and **3**.

DISCUSSION

There are several structure/function theories that have guided studies of PLM and related regulatory partners of transport ATPases. The first is that the oligomeric species of the regulatory peptide is a “storage” form that does not bind to the target ATPase. This model predicts that depolymerization of the oligomer would result in increased availability of the peptide for interaction with the ATPase enhancing the “apparent” affinity, reflected by a decrease K_d . The analogous regulatory protein phospholamban mostly fulfills this prediction^{39, 41}, and our previous studies with PLM phosphorylation site mutants also suggested that oligomerization was a major determinant of NKA-binding¹⁸. In that study we found that oligomerization and NKA-binding were inversely regulated by phosphorylation-mimicking mutations at sites of PKA/PKC functional regulation. Here we confirm that previous observation, compared to nonphosphorylatable mutant S63A/S68A the phosphomimetic mutant S63E/S68E shows increased oligomerization and a loss of NKA-binding (Fig. 2). However, our present more extensive survey of the PLM primary sequence also revealed several mutants that bind avidly to NKA yet are more oligomeric than WT (L33A, G31A, I26A, I23A) and a mutant that binds poorly to NKA but has an oligomerization dissociation constant that is the same as WT (I22A). Thus, we observed that the PLM mutants’ propensity for oligomerization was a very poor predictor of NKA binding.

The second assumption tested here was that increased binding to NKA results in increased pump inhibition. Notably, many of the 19 PLM mutants tested here showed more avid NKA-binding than WT (**Fig. 2B**), suggesting that the NKA-PLM interaction has been tuned for less than maximal binding. The observed increase in apparent affinity recommends these mutants as possible superinhibitors of NKA. However, 2 of the 3 mutants selected for further study did not yield the expected physiological effect in isolated cardiomyocytes. Only one (L30A) showed signs of enhanced inotropic potency in cultured adult cardiac myocytes (**Fig. 4**). The apparent disconnect between binding and functional inhibition reminds us

of another group's recent discovery of a small transmembrane peptide (DWORF) that appears to bind SERCA without inhibition⁴⁷. The data indicate that a gain of binding does not always yield a gain of inhibitory function. Likely the inverse is also true; perhaps some mutants that showed normal or decreased binding to NKA are still potent inhibitors of the pump. We conclude rationally designed modifications of regulatory proteins must be tested to verify that they have achieved the intended effect.

The discovery of L30A as a gain-of-binding (**Fig. 2B**) and superinhibitory (**Fig. 4**) mutant may be a useful observation in the search for alternatives to conventional cardiac glycoside therapy. The enhanced Ca^{2+} handling and contractility are reminiscent of the action of clinically useful NKA inhibitors on isolated cardiomyocytes (45-48). Specifically, L30A PLM overexpression increased the amplitude of the Ca^{2+} transient and decay constant (**Fig. 4C, H, J**) and increased the duration of the contraction (FWHM) (**Fig. 4F, L, M**). The respective mechanisms of contractility modulation by cardiac glycosides and superinhibitory PLM are contrasted in **Fig. 5**. Cardiac glycosides inhibit a fraction of the NKA pumps (1). With fewer active pumps, $[\text{Na}^+]_i$ rises (2), inhibiting normal NCX extrusion of Ca^{2+} (3). In the context of heart failure, this accumulation of Ca^{2+} increases SR Ca^{2+} load and improves cardiac contractility. However, $[\text{Na}^+]_i$ is already elevated in heart failure^{48, 49}, and arrhythmias can be induced by excessive $[\text{Na}^+]_i$ and by SR Ca^{2+} overload (4). Clinically, this is avoided by careful titration of the glycoside dose, but pharmacological NKA inhibition is not acutely regulated with responsiveness to stress. In contrast, the inhibition of NKA by PLM is dynamically regulated (**Fig. 5B**). Even superinhibition by L30A PLM appeared to be reversed by phosphorylation, as we observed that Ca^{2+} handling and cell shortening transients of WT- and superinhibitory L30A-expressing cells converged after β -adrenergic stimulation. In addition, PLM decreases the activity of NKA by decreasing Na^+ affinity (increasing K_{Na}) while preserving V_{max} ²⁰. Thus, a rise in $[\text{Na}^+]_i$ is limited by reserve NKA activity.

The present results provide insight into the importance of PLM transmembrane residues in determining PLM regulatory interactions with itself (oligomerization) and with NKA. Modification of these residues may tune the inhibitory potency of PLM by altering the amount of monomeric PLM available to interact with NKA (**Fig. 2A**), or by altering the intrinsic affinity of the monomer for the

regulatory target (Fig. 2B), or by changing the intrinsic inhibitory potency of PLM (Fig. 4). Finally, the results underscore the value of identifying superinhibitory variants of PLM that could be useful for increasing contractility while still retaining physiological reversibility during stress (**Fig. 5B**).

Acknowledgements: The authors are grateful for technical assistance from Dr. Daniel Blackwell, Aimee Bueno, Jollyn Tyryfter, Alex Ticho, Chris Stefonowicz, Daphne Xiaoqiong Dong, Dr. Liubov Brueggemann and Dr. Ken Byron. We also thank Dr. Jody Martin for production of adenoviral constructs and Dr. Aleksey Zima and Dr. Elisa Bovo for providing rabbit adult ventricular cardiomyocytes.

REFERENCES

- [1] McMurray, J. J., and Pfeffer, M. A. (2005) Heart failure, *Lancet* 365, 1877-1889.
- [2] Mudd, J. O., and Kass, D. A. (2008) Tackling heart failure in the twenty-first century, *Nature* 451, 919-928.
- [3] Go, A. S., Mozaffarian, D., Roger, V. L., Benjamin, E. J., Berry, J. D., Blaha, M. J., Dai, S., Ford, E. S., Fox, C. S., Franco, S., Fullerton, H. J., Gillespie, C., Hailpern, S. M., Heit, J. A., Howard, V. J., Huffman, M. D., Judd, S. E., Kissela, B. M., Kittner, S. J., Lackland, D. T., Lichtman, J. H., Lisabeth, L. D., Mackey, R. H., Magid, D. J., Marcus, G. M., Marelli, A., Matchar, D. B., McGuire, D. K., Mohler, E. R., 3rd, Moy, C. S., Mussolino, M. E., Neumar, R. W., Nichol, G., Pandey, D. K., Paynter, N. P., Reeves, M. J., Sorlie, P. D., Stein, J., Towfighi, A., Turan, T. N., Virani, S. S., Wong, N. D., Woo, D., Turner, M. B., American Heart Association Statistics, C., and Stroke Statistics, S. (2014) Heart disease and stroke statistics--2014 update: a report from the American Heart Association, *Circulation* 129, e28-e292.
- [4] Fuller, W., Tulloch, L. B., Shattock, M. J., Calaghan, S. C., Howie, J., and Wypijewski, K. J. (2013) Regulation of the cardiac sodium pump, *Cell Mol Life Sci* 70, 1357-1380.
- [5] Hauptman, P. J., and Kelly, R. A. (1999) Digitalis, *Circulation* 99, 1265-1270.
- [6] Yang, E. H., Shah, S., and Criley, J. M. (2012) Digitalis toxicity: a fading but crucial complication to recognize, *Am J Med* 125, 337-343.
- [7] Lingrel, J. B., Arguello, J. M., Van Huysse, J., and Kuntzweiler, T. A. (1997) Cation and cardiac glycoside binding sites of the Na,K-ATPase, *Ann N Y Acad Sci* 834, 194-206.
- [8] Philipson, K. D., and Nicoll, D. A. (2000) Sodium-calcium exchange: a molecular perspective, *Annu Rev Physiol* 62, 111-133.
- [9] Shattock, M. J., Ottolia, M., Bers, D. M., Blaustein, M. P., Boguslavskyi, A., Bossuyt, J., Bridge, J. H., Chen-Izu, Y., Clancy, C. E., Edwards, A., Goldhaber, J., Kaplan, J., Lingrel, J. B., Pavlovic, D., Philipson, K., Sipido, K. R., and Xie, Z. J. (2015) Na⁺/Ca²⁺ exchange and Na⁺/K⁺-ATPase in the heart, *J Physiol* 593, 1361-1382.
- [10] Bossuyt, J., Despa, S., Han, F., Hou, Z., Robia, S. L., Lingrel, J. B., and Bers, D. M. (2009) Isoform specificity of the Na/K-ATPase association and regulation by phospholemman, *J Biol Chem* 284, 26749-26757.
- [11] Cheung, J. Y., Zhang, X. Q., Song, J., Gao, E., Rabinowitz, J. E., Chan, T. O., and Wang, J. (2010) Phospholemman: a novel cardiac stress protein, *Clin Transl Sci* 3, 189-196.
- [12] Bossuyt, J., Despa, S., Martin, J. L., and Bers, D. M. (2006) Phospholemman phosphorylation alters its fluorescence resonance energy transfer with the Na/K-ATPase pump, *J Biol Chem* 281, 32765-32773.
- [13] Cheung, J. Y., Zhang, X. Q., Song, J., Gao, E., Chan, T. O., Rabinowitz, J. E., Koch, W. J., Feldman, A. M., and Wang, J. (2013) Coordinated regulation of cardiac Na⁽⁺⁾/Ca⁽²⁺⁾ exchanger and Na⁽⁺⁾-K⁽⁺⁾-ATPase by phospholemman (FXD1), *Adv Exp Med Biol* 961, 175-190.
- [14] Wanichawan, P., Hodne, K., Hafver, T. L., Lunde, M., Martinsen, M., Louch, W. E., Sejersted, O. M., and Carlson, C. R. (2016) Development of a high-affinity peptide that prevents phospholemman (PLM) inhibition of the sodium/calcium exchanger 1 (NCX1), *Biochem J* 473, 2413-2423.
- [15] Hafver, T. L., Hodne, K., Wanichawan, P., Aronsen, J. M., Dalhus, B., Lunde, P. K., Lunde, M., Martinsen, M., Enger, U. H., Fuller, W., Sjaastad, I., Louch, W. E., Sejersted, O. M., and Carlson, C. R. (2016) Protein Phosphatase 1c Associated with the Cardiac Sodium

- Calcium Exchanger 1 Regulates Its Activity by Dephosphorylating Serine 68-phosphorylated Phospholemman, *J Biol Chem* 291, 4561-4579.
- [16] Beevers, A. J., and Kukol, A. (2006) Secondary structure, orientation, and oligomerization of phospholemman, a cardiac transmembrane protein, *Protein Sci* 15, 1127-1132.
- [17] Boguslavskiy, A., Pavlovic, D., Aughton, K., Clark, J. E., Howie, J., Fuller, W., and Shattock, M. J. (2014) Cardiac hypertrophy in mice expressing unphosphorylatable phospholemman, *Cardiovasc Res* 104, 72-82.
- [18] Song, Q., Pallikkuth, S., Bossuyt, J., Bers, D. M., and Robia, S. L. (2011) Phosphomimetic mutations enhance oligomerization of phospholemman and modulate its interaction with the Na/K-ATPase, *J Biol Chem* 286, 9120-9126.
- [19] Wypijewski, K. J., Howie, J., Reilly, L., Tulloch, L. B., Aughton, K. L., McLatchie, L. M., Shattock, M. J., Calaghan, S. C., and Fuller, W. (2013) A separate pool of cardiac phospholemman that does not regulate or associate with the sodium pump: multimers of phospholemman in ventricular muscle, *J Biol Chem* 288, 13808-13820.
- [20] Despa, S., Bossuyt, J., Han, F., Ginsburg, K. S., Jia, L. G., Kutchai, H., Tucker, A. L., and Bers, D. M. (2005) Phospholemman-phosphorylation mediates the beta-adrenergic effects on Na/K pump function in cardiac myocytes, *Circ Res* 97, 252-259.
- [21] Bidwell, P., Blackwell, D. J., Hou, Z., Zima, A. V., and Robia, S. L. (2011) Phospholamban binds with differential affinity to calcium pump conformers, *J Biol Chem* 286, 35044-35050.
- [22] Khafaga, M., Bossuyt, J., Mamikonian, L., Li, J. C., Lee, L. L., Yarov-Yarovoy, V., Despa, S., and Bers, D. M. (2012) Na(+)/K(+)-ATPase E960 and phospholemman F28 are critical for their functional interaction, *Proc Natl Acad Sci U S A* 109, 20756-20761.
- [23] Blackman, S. M., Piston, D. W., and Beth, A. H. (1998) Oligomeric state of human erythrocyte band 3 measured by fluorescence resonance energy homotransfer, *Biophys J* 75, 1117-1130.
- [24] Zal, T., and Gascoigne, N. R. (2004) Photobleaching-corrected FRET efficiency imaging of live cells, *Biophys J* 86, 3923-3939.
- [25] Beevers, A. J., and Kukol, A. (2007) Phospholemman transmembrane structure reveals potential interactions with Na⁺/K⁺-ATPase, *J Biol Chem* 282, 32742-32748.
- [26] Hess, B., Kutzner, C., van der Spoel, D., and Lindahl, E. (2008) GROMACS 4: Algorithms for highly efficient, load-balanced, and scalable molecular simulation, *Journal of Chemical Theory and Computation* 4, 435-447.
- [27] Pronk, S., Pall, S., Schulz, R., Larsson, P., Bjelkmar, P., Apostolov, R., Shirts, M. R., Smith, J. C., Kasson, P. M., van der Spoel, D., Hess, B., and Lindahl, E. (2013) GROMACS 4.5: a high-throughput and highly parallel open source molecular simulation toolkit, *Bioinformatics* 29, 845-854.
- [28] Huang, J., and MacKerell, A. D., Jr. (2013) CHARMM36 all-atom additive protein force field: validation based on comparison to NMR data, *J Comput Chem* 34, 2135-2145.
- [29] Jorgensen, W. L., Chandrasekhar, J., Madura, J. D., Impey, R. W., and Klein, M. L. (1983) Comparison of Simple Potential Functions for Simulating Liquid Water, *Journal of Chemical Physics* 79, 926-935.
- [30] Darden, T., York, D., and Pedersen, L. (1993) Particle Mesh Ewald - an N.LOG(N) Method for Ewald Sums in Large Systems, *Journal of Chemical Physics* 98, 10089-10092.
- [31] Essmann, U., Perera, L., Berkowitz, M. L., Darden, T., Lee, H., and Pedersen, L. G. (1995) A Smooth Particle Mesh Ewald Method, *Journal of Chemical Physics* 103, 8577-8593.

- [32] Berendsen, H. J. C., Postma, J. P. M., Vangunsteren, W. F., Dinola, A., and Haak, J. R. (1984) Molecular-Dynamics with Coupling to an External Bath, *Journal of Chemical Physics* 81, 3684-3690.
- [33] Hoover, W. G. (1985) Canonical Dynamics - Equilibrium Phase-Space Distributions, *Phys. Rev. A* 31, 1695-1697.
- [34] Nose, S. (1984) A Molecular-Dynamics Method for Simulations in the Canonical Ensemble, *Mol. Phys.* 52, 255-268.
- [35] Nose, S., and Klein, M. L. (1983) Constant Pressure Molecular-Dynamics for Molecular-Systems, *Mol. Phys.* 50, 1055-1076.
- [36] Parrinello, M., and Rahman, A. (1981) Polymorphic Transitions in Single-Crystals - a New Molecular-Dynamics Method, *J. Appl. Phys.* 52, 7182-7190.
- [37] Domeier, T. L., Blatter, L. A., and Zima, A. V. (2009) Alteration of sarcoplasmic reticulum Ca²⁺ release termination by ryanodine receptor sensitization and in heart failure, *J Physiol* 587, 5197-5209.
- [38] Mishra, N. K., Habeck, M., Kirchner, C., Haviv, H., Peleg, Y., Eisenstein, M., Apell, H. J., and Karlish, S. J. (2015) Molecular Mechanisms and Kinetic Effects of FX₁YD1 and Phosphomimetic Mutants on Purified Human Na,K-ATPase, *J Biol Chem* 290, 28746-28759.
- [39] Hou, Z., Kelly, E. M., and Robia, S. L. (2008) Phosphomimetic mutations increase phospholamban oligomerization and alter the structure of its regulatory complex, *J Biol Chem* 283, 28996-29003.
- [40] Kelly, E. M., Hou, Z., Bossuyt, J., Bers, D. M., and Robia, S. L. (2008) Phospholamban oligomerization, quaternary structure, and sarco(endo)plasmic reticulum calcium ATPase binding measured by fluorescence resonance energy transfer in living cells, *J Biol Chem* 283, 12202-12211.
- [41] Kimura, Y., Kurzydowski, K., Tada, M., and MacLennan, D. H. (1997) Phospholamban inhibitory function is activated by depolymerization, *J Biol Chem* 272, 15061-15064.
- [42] Altamirano, J., Li, Y., DeSantiago, J., Piacentino, V., 3rd, Houser, S. R., and Bers, D. M. (2006) The inotropic effect of cardioactive glycosides in ventricular myocytes requires Na⁺-Ca²⁺ exchanger function, *J Physiol* 575, 845-854.
- [43] Bers, D. M. (1987) Mechanisms contributing to the cardiac inotropic effect of Na pump inhibition and reduction of extracellular Na, *J Gen Physiol* 90, 479-504.
- [44] Bers, D. M. (2002) Cardiac excitation-contraction coupling, *Nature* 415, 198-205.
- [45] Bers, D. M., and Bridge, J. H. (1988) Effect of acetylstrophanthidin on twitches, microscopic tension fluctuations and cooling contractures in rabbit ventricle, *J Physiol* 404, 53-69.
- [46] Waggoner, J. R., Ginsburg, K. S., Mitton, B., Haghghi, K., Robbins, J., Bers, D. M., and Kranias, E. G. (2009) Phospholamban overexpression in rabbit ventricular myocytes does not alter sarcoplasmic reticulum Ca transport, *Am J Physiol Heart Circ Physiol* 296, H698-703.
- [47] Nelson, B. R., Makarewich, C. A., Anderson, D. M., Winders, B. R., Troupes, C. D., Wu, F., Reese, A. L., McAnally, J. R., Chen, X., Kavalali, E. T., Cannon, S. C., Houser, S. R., Bassel-Duby, R., and Olson, E. N. (2016) A peptide encoded by a transcript annotated as long noncoding RNA enhances SERCA activity in muscle, *Science* 351, 271-275.

- [48] Despa, S., Islam, M. A., Weber, C. R., Pogwizd, S. M., and Bers, D. M. (2002) Intracellular Na(+) concentration is elevated in heart failure but Na/K pump function is unchanged, *Circulation* 105, 2543-2548.
- [49] Piacentino, V., 3rd, Weber, C. R., Chen, X., Weisser-Thomas, J., Margulies, K. B., Bers, D. M., and Houser, S. R. (2003) Cellular basis of abnormal calcium transients of failing human ventricular myocytes, *Circ Res* 92, 651-658.

TABLES

Table 1. Results of fitting acceptor sensitization FRET and anisotropy data with Hill functions. The fitting parameters for each PLM mutant are listed \pm SEM. $N \geq 4$ biological replicates.

PLM Mutant	r_0	r_n	K_D1	n	c (%)	FRET _{max} (%)	K_D2	n
WT	0.212 \pm 0.001	0.092 \pm 0.003	2.19 \pm 0.18	1.20 \pm 0.06	-0.8 \pm 0.3	54.7 \pm 2.1	9.9 \pm 1.4	0.79 \pm 0.03
S63E/S68E	0.253 \pm 0.003	0.067 \pm 0.004	1.31 \pm 0.14	0.70 \pm 0.03	-0.1 \pm 0.1	58.9 \pm 2.1	14.0 \pm 1.1	0.75 \pm 0.02
S36A/S68A	0.271 \pm 0.004	0.052 \pm 0.008	1.96 \pm 0.20	0.51 \pm 0.03	0.7 \pm 0.1	44.4 \pm 0.7	5.5 \pm 0.3	1.06 \pm 0.02
S37A	0.213 \pm 0.002	0.064 \pm 0.007	2.69 \pm 0.20	0.80 \pm 0.06	0.6 \pm 0.3	35.2 \pm 1.4	3.9 \pm 0.2	1.00 \pm 0.05
I36A	0.245 \pm 0.004	0.061 \pm 0.009	2.16 \pm 0.23	0.68 \pm 0.05	0.6 \pm 0.2	32.7 \pm 0.8	3.3 \pm 0.1	1.13 \pm 0.04
V35A	0.234 \pm 0.004	0.066 \pm 0.009	1.94 \pm 0.25	0.67 \pm 0.06	0.6 \pm 0.3	39.3 \pm 1.7	3.7 \pm 0.2	1.01 \pm 0.05
I34A	0.215 \pm 0.002	0.089 \pm 0.004	1.94 \pm 0.12	1.12 \pm 0.07	0.1 \pm 0.2	40.9 \pm 1.3	4.0 \pm 0.3	1.05 \pm 0.04
L33A	0.249 \pm 0.003	0.069 \pm 0.007	1.52 \pm 0.08	0.71 \pm 0.04	0.4 \pm 0.1	31.3 \pm 0.7	3.0 \pm 0.1	1.18 \pm 0.03
I32A	0.232 \pm 0.001	0.082 \pm 0.004	1.80 \pm 0.09	1.07 \pm 0.05	0.7 \pm 0.1	28.3 \pm 0.4	2.5 \pm 0.2	1.40 \pm 0.04
G31A	0.263 \pm 0.003	0.081 \pm 0.000	1.41 \pm 0.17	0.67 \pm 0.02	1.4 \pm 0.1	22.6 \pm 0.7	2.8 \pm 0.1	1.41 \pm 0.06
L30A	0.287 \pm 0.015	-0.044 \pm 0.063	8.20 \pm 1.19	0.35 \pm 0.07	1.4 \pm 0.2	26.9 \pm 0.7	2.7 \pm 0.1	1.22 \pm 0.06
I29A	0.251 \pm 0.006	0.048 \pm 0.019	2.67 \pm 0.22	0.59 \pm 0.07	1.7 \pm 0.2	25.8 \pm 0.8	2.9 \pm 0.2	1.35 \pm 0.07
F28A	0.214 \pm 0.002	0.085 \pm 0.007	2.97 \pm 0.26	1.00 \pm 0.09	1.2 \pm 0.3	30.8 \pm 0.8	2.8 \pm 0.1	1.23 \pm 0.07
L27A	0.236 \pm 0.003	0.067 \pm 0.012	2.87 \pm 0.30	0.79 \pm 0.08	0.9 \pm 0.2	23.9 \pm 0.9	3.1 \pm 0.1	1.12 \pm 0.07
I26A	0.272 \pm 0.006	0.063 \pm 0.018	1.52 \pm 0.13	0.65 \pm 0.08	1.1 \pm 0.1	36.0 \pm 1.8	4.7 \pm 0.4	1.04 \pm 0.05
G25A	0.244 \pm 0.004	0.073 \pm 0.011	2.13 \pm 0.18	0.71 \pm 0.07	0.9 \pm 0.1	31.8 \pm 0.8	3.7 \pm 0.2	1.08 \pm 0.04
I23A	0.257 \pm 0.003	0.084 \pm 0.008	1.65 \pm 0.10	0.79 \pm 0.06	0.8 \pm 0.1	40.1 \pm 1.0	5.4 \pm 0.3	1.09 \pm 0.02
I22A	0.265 \pm 0.004	0.055 \pm 0.014	2.22 \pm 0.17	0.62 \pm 0.06	0.0 \pm 0.1	58.9 \pm 2.8	17.2 \pm 1.1	0.77 \pm 0.02
L21A	0.258 \pm 0.005	0.047 \pm 0.024	3.04 \pm 0.25	0.66 \pm 0.08	0.6 \pm 0.1	50.1 \pm 2.1	10.3 \pm 0.8	0.97 \pm 0.03
G20A	0.249 \pm 0.003	0.072 \pm 0.008	1.77 \pm 0.05	0.76 \pm 0.05	0.3 \pm 0.1	46.3 \pm 1.6	6.8 \pm 0.3	0.98 \pm 0.03
G19A	0.235 \pm 0.002	0.075 \pm 0.006	2.36 \pm 0.10	0.85 \pm 0.05	0.4 \pm 0.1	42.8 \pm 0.8	5.8 \pm 0.1	1.01 \pm 0.02
I18A	0.298 \pm 0.010	0.039 \pm 0.028	1.52 \pm 0.06	0.53 \pm 0.08	0.6 \pm 0.1	49.4 \pm 1.4	7.3 \pm 0.2	1.02 \pm 0.02

Table 2. Ca²⁺ transient data for WT vs. L30A-expressing cells displayed as means ± SEM. p-values from Student's T-Test are listed. N = 4 biological replicates comprising a total of 38 myocytes.

Parameter		WT		L30A	P-Value
Baseline Indo-1		0.444		0.431	
Ratio	±	0.008	±	0.003	0.139
Peak Indo-1		0.61		0.61	
Ratio	±	0.01	±	0.01	0.682
Transient Amplitude		0.22		0.26	
Transient Amplitude	±	0.01	±	0.01	0.036
Transient Amplitude		37		42	
(% of Baseline)	±	2	±	2	0.124
Departure Velocity		7.1		7.7	
(sec. ⁻¹)	±	0.4	±	0.4	0.331
Time to 10% Peak		0.080		0.100	
Time to 10% Peak	±	0.008	±	0.009	0.094
Time to 50% Peak		0.037		0.040	
Time to 50% Peak	±	0.001	±	0.002	0.231
Time to 90% Peak		0.093		0.092	
Time to 90% Peak	±	0.005	±	0.006	0.915
Time to Peak		0.20		0.23	
Time to Peak	±	0.01	±	0.01	0.193
Return Velocity		-0.30		-0.30	
Return Velocity	±	0.02	±	0.02	0.940
Time to 10% Baseline		0.43		0.46	
Time to 10% Baseline	±	0.02	±	0.03	0.387
Time to 50% Baseline		0.81		0.89	
Time to 50% Baseline	±	0.03	±	0.03	0.053
Time to 90% Baseline		1.42		1.52	
Time to 90% Baseline	±	0.04	±	0.02	0.027
Full Width at Half Maximum		0.77		0.85	
Full Width at Half Maximum	±	0.03	±	0.03	0.063
Ca ²⁺ Decay Time Constant		1.02		1.19	
Ca ²⁺ Decay Time Constant	±	0.07	±	0.05	0.045

Table 3. Myocyte contraction data for WT vs. L30A-expressing cells displayed as means \pm SEM. p-values from Student's T-Test are listed. N = 4 biological replicates comprising a total of 38 myocytes.

Parameter	WT	L30A	P-Value
Baseline Sarcomere Length (μm)	1.714 \pm 0.007	1.675 \pm 0.006	<0.001
Length at Peak Contraction (μm)	1.584 \pm 0.009	1.559 \pm 0.006	0.023
Change in Length (μm)	0.130 \pm 0.006	0.116 \pm 0.005	0.086
Fractional Shortening (%)	7.6 \pm 0.4	6.9 \pm 0.3	0.148
Contraction Velocity ($\mu\text{m}/\text{sec.}$)	-0.51 \pm 0.04	-0.37 \pm 0.03	0.007
Time to 10% Peak (sec.)	0.072 \pm 0.004	0.085 \pm 0.008	0.161
Time to 50% Peak (sec.)	0.201 \pm 0.009	0.233 \pm 0.009	0.013
Time to 90% Peak (sec.)	0.47 \pm 0.02	0.53 \pm 0.02	0.017
Time to Peak (sec.)	0.68 \pm 0.03	0.81 \pm 0.02	0.001
Relaxation Velocity ($\mu\text{m}/\text{sec.}$)	0.61 \pm 0.08	0.39 \pm 0.05	0.018
Time to 10% Baseline (sec.)	0.84 \pm 0.03	1.02 \pm 0.03	<0.001
Time to 50% Baseline (sec.)	1.00 \pm 0.04	1.22 \pm 0.03	<0.001
Time to 90% Baseline (sec.)	1.22 \pm 0.05	1.45 \pm 0.03	<0.001
Full Width at Half Maximum (sec.)	0.80 \pm 0.04	0.99 \pm 0.03	<0.001
Relaxation Time Constant (sec.)	0.40 \pm 0.03	0.56 \pm 0.04	0.002

FIGURE LEGENDS

Figure 1. Method for measuring PLM-PLM and PLM-NKA binding. (A) Primary amino acid sequences of the human and canine isoforms of PLM. The N-terminal residues (including the underlined FXYD motif) are extracellular and the C-terminal residues (including the phosphorylation sites, in boxes) are intracellular. The single transmembrane domain is highlighted in gray. For the current study the canine isoform was used. (B) PLM forms tetramers in the plasma membrane, and PLM monomer binds to and inhibits NKA. (C) HEK cells stably expressing ECFP-NKA (left), transiently transfected with PLM-Cit (center), and stained with WGA Alexa Fluor 594 (right). (D) The average acceptor sensitization FRET efficiency of each cell co-transfected with ECFP-NKA and WT PLM-Cit, and (E) the average anisotropy of PLM-Cit are plotted against the intensity of Cit in arbitrary units (AU) as an index of [PLM]. Each point is derived from one cell. The data were fit with Hill functions shown in red.

Figure 2. Effects of alanine substitution on PLM-PLM and PLM-NKA binding affinities. (A) For each PLM mutant, K_D1 is plotted in arbitrary units (AU) \pm SEM and compared to WT (dashed line). Mutants with K_D1 less than the K_D1 for WT are considered more oligomeric (greater PLM-PLM binding affinity) and mutants with a greater K_D1 are considered less oligomeric. (B) K_D2 is plotted in arbitrary units (AU) \pm SEM for each mutant, and compared to WT (dashed line). Mutants with K_D2 less than WT are considered gain-of-binding, and mutants with a greater K_D2 are considered loss-of-binding. * $p < 0.05$ compared to WT.

Figure 3. Molecular dynamics simulations of WT and L30A tetramer structure models. (A) A comparison of the initial (start) and final (10 ns) tetramer structures, with the leu (WT) or ala (L30A) residues highlighted in blue. We observed significant distortion of the L30A tetramer during the simulation. (B) A histogram of potential energy values of structures sampled during the simulation reveals that the energy of the L30A PLM tetramer is increased compared to WT, suggesting decreased stability for the mutant structure.

Figure 4. Functional effects of PLM mutants in myocytes. (A) A rabbit ventricular myocyte infected with adenovirus used to express PLM-Cit. The protein is synthesized in the SR and trafficked to the sarcolemma and T-tubules, as evidenced by co-localization with WGA Alexa Fluor 594. (B) Averaged Ca^{2+} transients for myocytes overexpressing WT PLM (black) and GFP (red) are plotted as the normalized fluorescence ratio of Indo-1 over time, \pm SEM. (C) Ca^{2+} transients for WT (black) vs. L30A PLM (red). (D) Same as C, but in the presence of 20 nM isoproterenol. (E) The myocyte contractions corresponding to the experiment in B. (F) Myocyte contractions corresponding to the experiment in C. (G) The myocyte contractions corresponding to the experiment in D. Values in E-G are mean \pm SEM. (H) Averaged Ca^{2+} transient amplitude. (I) Ca^{2+} transient full width at half maximum. (J) Ca^{2+} decay time constant. (K) Fractional shortening. (L) Full width at half maximum for cell contractions. (M) Cell relaxation time constant. Values in H-M are mean \pm SEM, normalized to WT, * indicates $p < 0.05$ compared to WT.

Figure 5. Pharmacological vs. physiological inhibition of NKA. (A) Cardiac glycosides act by binding to and inhibiting the activity of NKA in the sarcolemma of cardiomyocytes (1). This leads to an increase in $[Na^+]_i$, which inhibits the ability of NCX to extrude calcium (2). As calcium rises in the cytosol and in the SR (3), contractility is increased as intended. However, overdose of cardiac glycosides leads to overload of calcium in the SR and leakage out of the SR, potentially causing an arrhythmia (4). (B) In this study, L30A PLM displayed increased binding to NKA (compared to WT PLM), and mimicked the effects of cardiac glycosides on isolated cardiomyocytes. Following β -adrenergic stimulation, which is known to cause PLM phosphorylation, there were no differences between WT- and L30A-overexpressing cells, suggesting that the effect of L30A mutation was physiologically reversible.

Figure 1

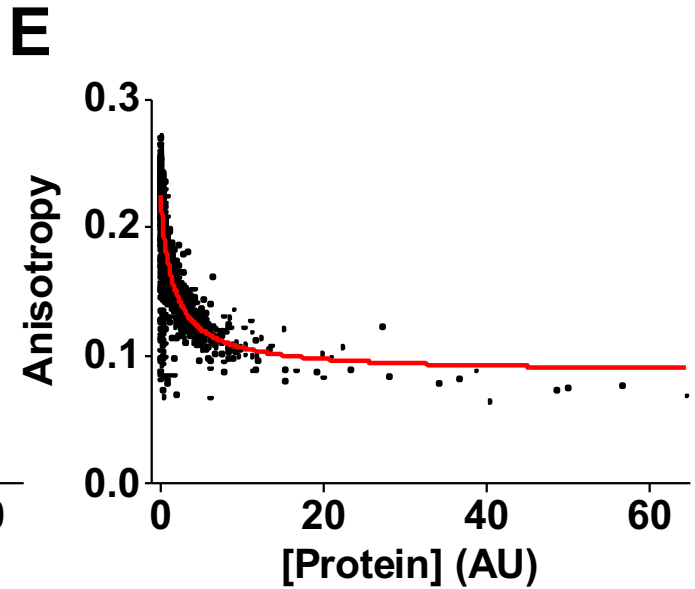
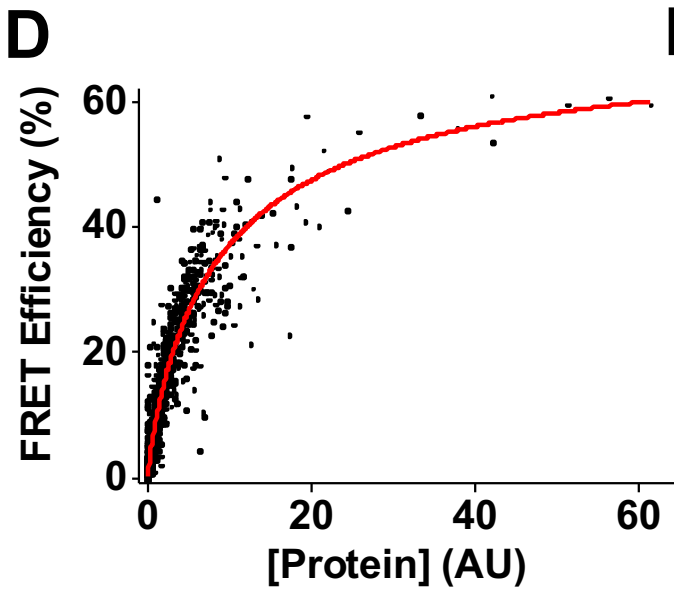
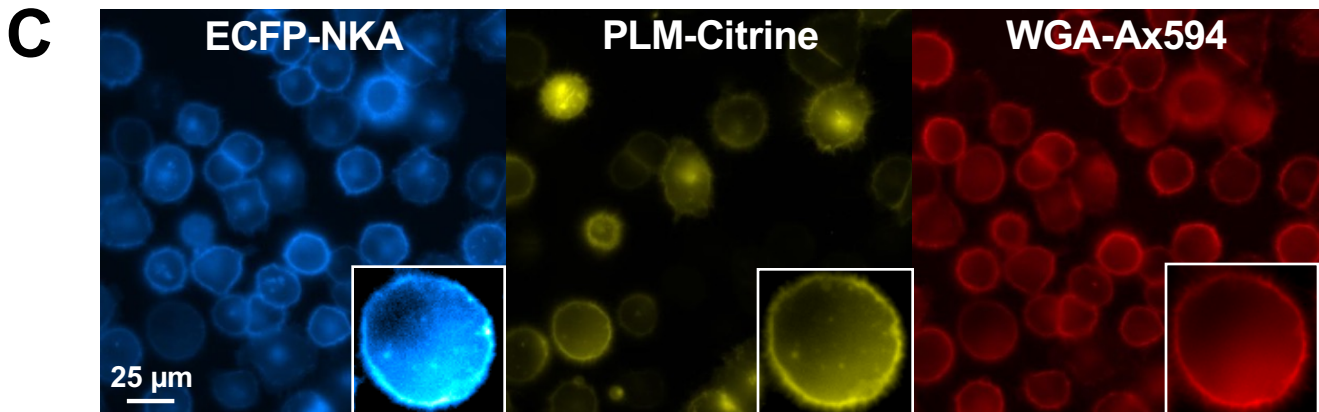
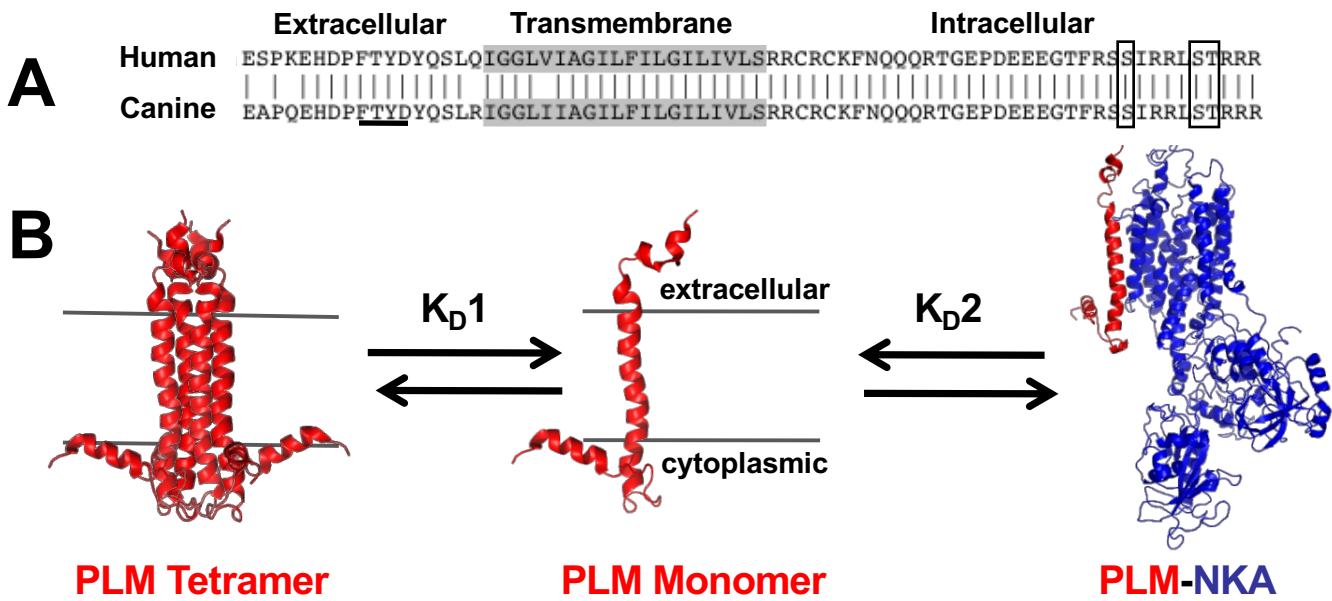
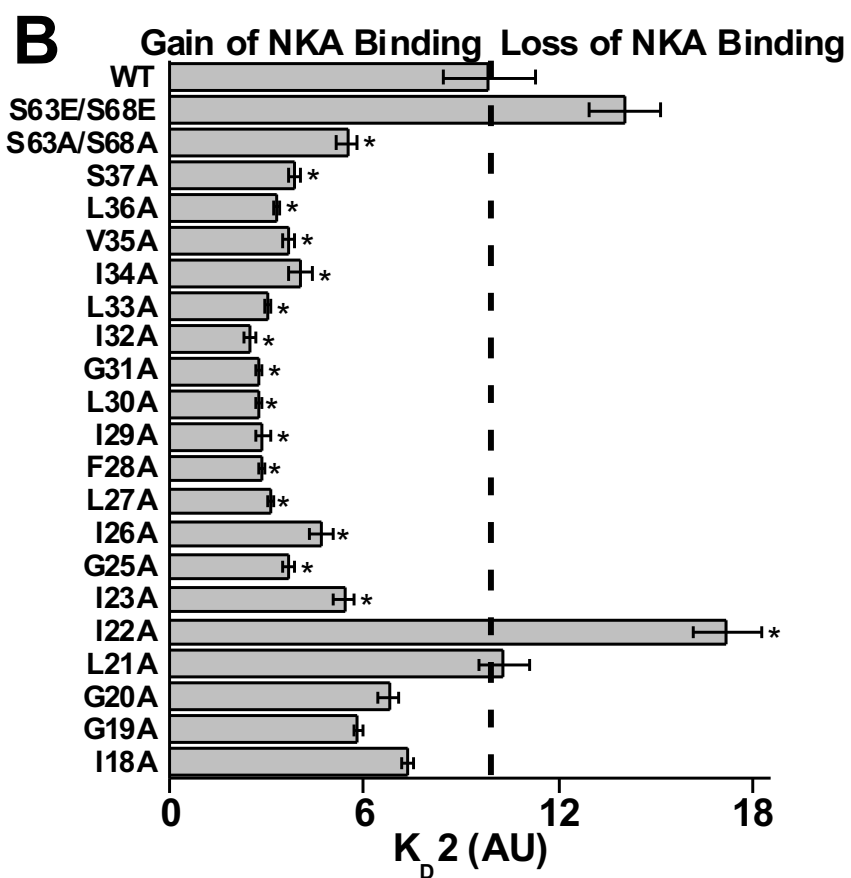
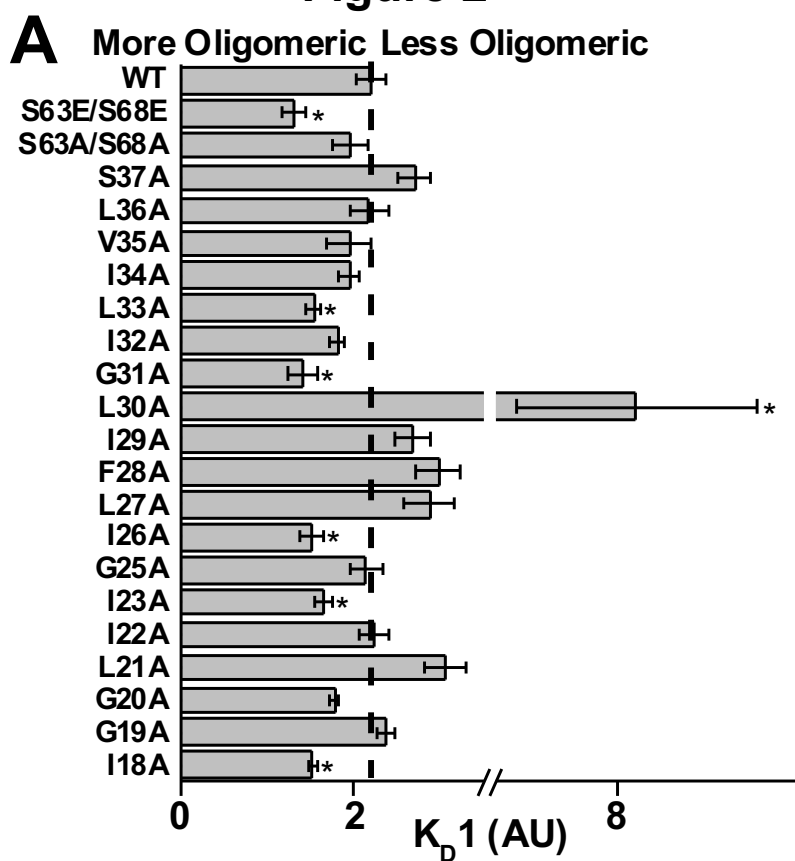


Figure 2



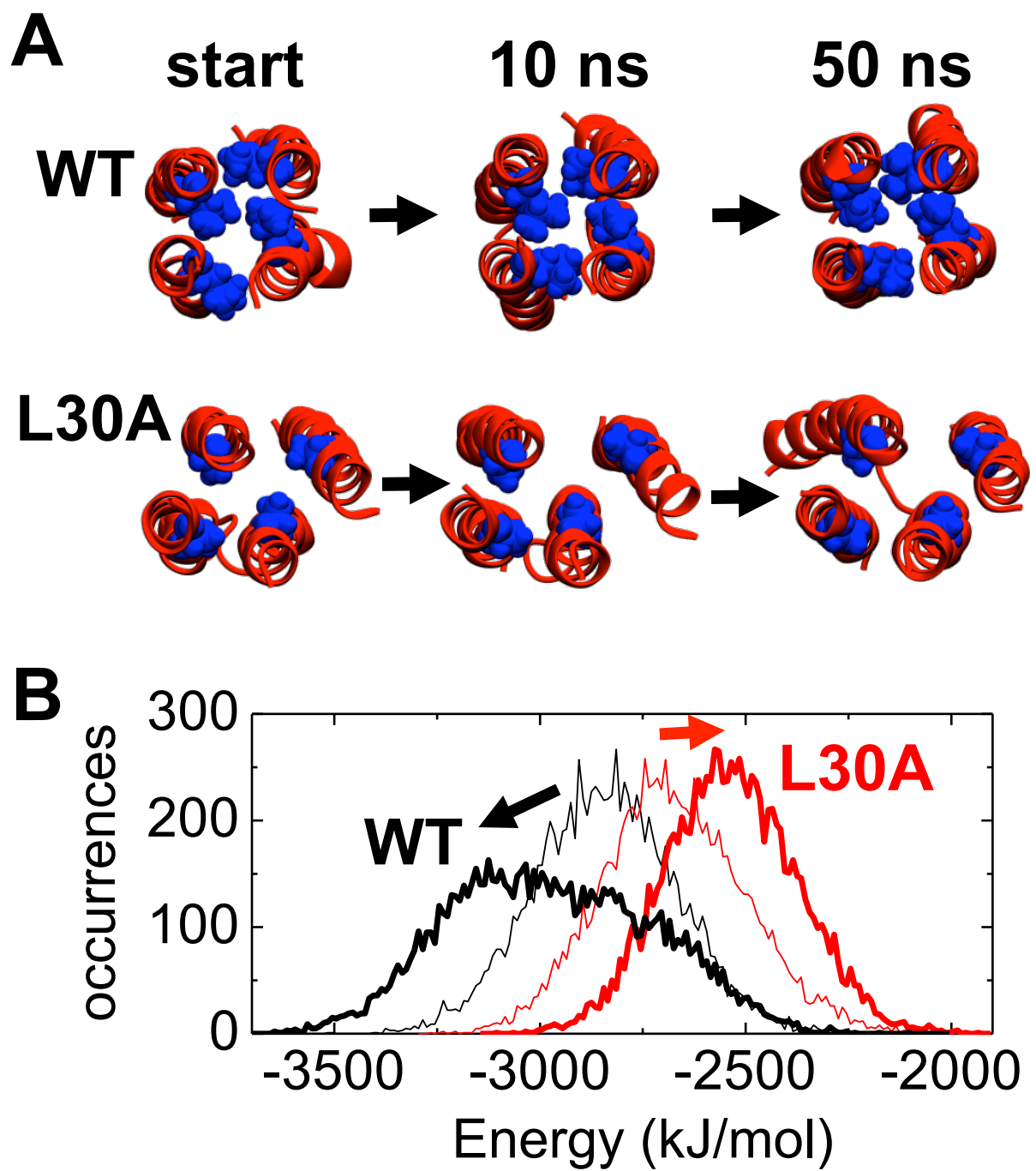


Figure 4

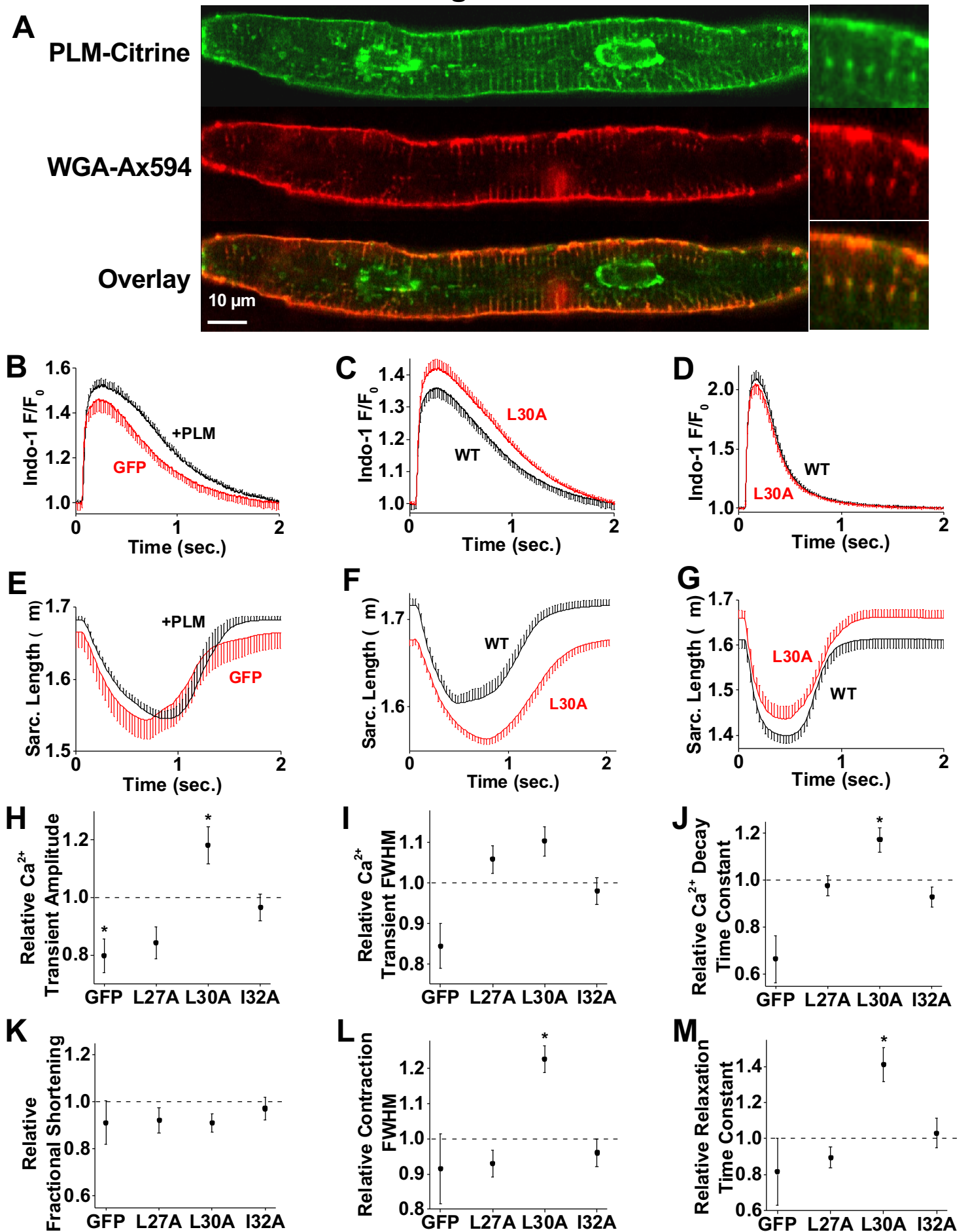
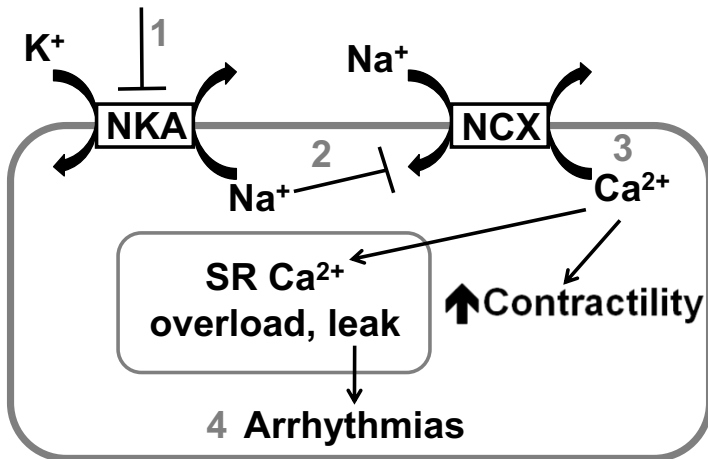


Figure 5

A *Pharmacological NKA Inhibition*
Cardiac Glycosides



B *Physiological NKA Inhibition*

